SCIENTIFIC REPORTS

OPEN

Received: 18 June 2018
Accepted: 30 November 2018
Published online: 04 February 2019

# Revealing Solid Properties of High-energy-density Molecular Cocrystals from the Cooperation of Hydrogen Bonding and Molecular Polarizability

Lei Zhang[1,2], Sheng-Li Jiang[1], Yi Yu[1] & Jun Chen[1,2,3]

**In the domain of high-energy-density materials, the understanding to physico-chemical properties has long been primarily based on molecular structures whereas the crystal packing effect that significantly affects solid properties has been seldom involved. Herewith we predict the solid properties of six novel energetic cocrystals by taking into account of the crystal packing effect using a quantum chemistry method. We discover that the hydrogen bonding causes an increase in the molecular polarizability and their cooperation significantly changes the solid-state nature of the cocrystals compared to the pristine crystal and the gas counterparts. For example, stabilizing the multi-component molecular association by increasing the binding energy by 19–41% over the pristine crystals, improving the detonation performance by 5–10% and reducing the sensitivity to external stimuli compared to their pure crystal or gas counterparts. Therefore, the solid nature of the cocrystal is not a simple combination of the pure crystalline properties of its components and the heterogeneous molecular coupling effects must be considered to design improved functional cocrystals.**

Cocrystallization, tailoring crystal packing effects by intermolecular charge transfer and intramolecular charge redistribution, has been supposed to be an effective way to tune the nature of functional materials over their pristine counterparts[1–6]. In designing improved high-energy-density materials, a key goal is to achieve an optimum balance between two inherently contradictory objectives: a high level of detonation performance and low sensitivity to accidental initiation of detonation[7,8]. The introduction of cocrystallization technology into energetic materials domain has given us hope to break the dilemma[1,9,10]. For example, using high-energy-density hexanitrohexaazaisowurtzitane molecule (CL-20, $C_6H_6N_{12}O_{12}$) and low-sensitivity octahydro-1,3,5,7-tetranitro-1,3,5,7-tetrazocine molecule (HMX, $C_4H_8N_8O_8$) as raw materials, the obtained 2:1 CL-20:HMX cocrystal has a firing power close to CL-20[11] and similar safety properties to HMX. By mixing CL-20 molecules and low-sensitivity 2,4,6-trinitrotoluene molecules (TNT, $C_7H_5N_3O_6$), 1:1 CL-20:TNT cocrystal has twice the stability of CL-20 and is safe enough to transport[12].

To effectively achieve the engineering of improved energetic cocrystals, the critical issues are how the multi-component molecules interact to stabilize the crystal structure and tune the solid nature. However, from years the quantum chemical understanding to physicochemical properties of high-energy-density crystals have been based solely on molecular structures[13–16]. Most of the researches were limited to the development of empirical quantitative structure-property relationships (QSPR) model based on the constitutional, topological, geometric, or quantum chemical descriptions of free molecules[8,17,18]. The crystal packing effect, although important and decisive to the solid properties, has been seldom involved[8,19–21].

[1]Software Centre for High Performance Numerical Simulation, Institute of Applied Physics and Computational Mathematics, Beijing, 100088, People's Republic of China. [2]Laboratory of Computational Physics, Institute of Applied Physics and Computational Mathematics, Beijing, 100088, People's Republic of China. [3]Center for Applied Physics and Technology, Peking University, Beijing, 100871, China. Lei Zhang and Sheng-Li Jiang contributed equally. Correspondence and requests for materials should be addressed to J.C. (email: Jun_chen@iapcm.ac.cn)

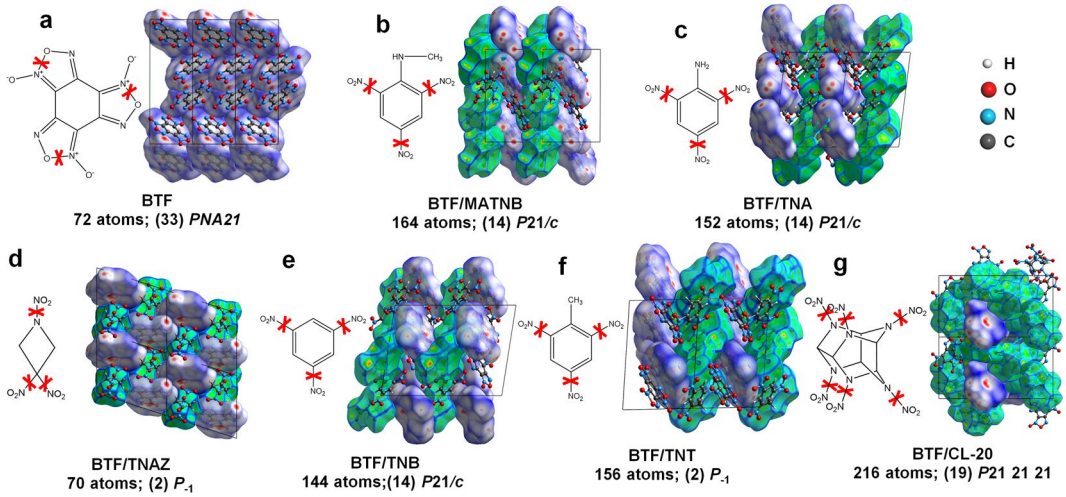


**Figure 1.** Chemical diagrams of high-energy-density molecules of BTF, MATNB, TNA, TNAZ, TNB, TNT, and CL-20; 3D crystal packing structures of pristine BTF crystal and BTF/MATNB, BTF/TNA, BTF/TNAZ, BTF/TNB, BTF/TNT, and BTF/CL-20 cocrystals. The domain of each individual molecule is illustrated by the corresponding Hirshfeld surface: the BTF molecule is enclosed by blue surfaces and the other molecules are enclosed by the green. The red-crosses denote the trigger linkages for chemical reaction initiation for each molecule.

To this end, we study the solid properties of six novel high-energy-density molecular cocrystals composed of benzotrifuroxan (BTF, $C_6N_6O_6$)[22,23], nitro compound molecules including 2,4,6-trinitrobenzene methylamine (MATNB, $C_7N_4O_6O_6$), 2,4,6-trinitroaniline (TNA, $C_6N_4O_6O_4$), 1,3,3-trinitroazetidine (TNAZ, $C_3N_4O_6O_4$), 1,3,5-Trinitrobenzene (TNB, $C_6N_3O_6O_3$), TNT, and nitroamine molecule CL-20. BTF is one of the most powerful explosives available in the commercial field currently, but it is sensitive to external stimuli. In the impact tests, the measured $h_{50\%}$ of BTF (21 *cm*[22] or 50 *cm*[8]) was significantly smaller than that of the insensitive explosive triaminotrinitrobenzene (TATB) (>320 *cm*[8]). Introducing hydrogen-containing component to the BTF molecules is expected to provide improved overall properties of the novel cocrystals, however, most of the properties cannot be obtained experimentally, because in addition to safety issues, the sample amount of the novel product is difficult to up to standard.

Herewith, using a quantum chemistry method, we predict the structural, thermodynamic, explosion and safety properties of a series of typical novel energetic cocrystals and evaluate the multicomponent molecular packing effect. An interesting coupling of hydrogen bonding and molecular polarizability and their effect in tuning the solid-state nature of the cocrystals is reported. Our work is expected to provide useful reference towards designing improved energetic-energetic cocrystals.

## Results and Discussion

**Repulsive inter-lone-pair interactions and Attractive proton-lone pair interaction.** Intermolecular charge transfer and intramolecular charge redistribution are observed in the structures of BTF, BTF/MATNB, BTF/TNA, BTF/TNAZ, BTF/TNB, BTF/TNT, and BTF/CL-20 due to the periodic packing of molecules in space, as shown in Figs 1 and 2. Such molecular packing introduces three types of intermolecular interactions for the close-confronting atoms – inter-lone-pair interactions, lone-pair-π interactions and proton-lone pair interactions (*i.e.* hydrogen bonding)[24–26].

BTF molecule consists of electronegative elements of oxygen and nitrogen, which have two pairs and one pair of lone-pair electrons, respectively. Thus, all the interactions within BTF crystal are inter-lone-pair interactions in addition to the aromatic stacking interactions (Fig. 2). According to the calculated crystal orbital Hamilton population (COHP), all the inter-lone-pair interactions (N···N, O···N, and O···O) and lone pair-π interactions (O···C) are antibonding and furnish each a positive item to the total energy, ranging from +0.69 *kcal/mol* to +1.15 *kcal/mol* (Table 1 and Supplementary Fig. S2). Therefore, in the equilibrium crystal structure, such inter-lone-pair and lone-pair-π interactions are mutually exclusive and serve to balance the *van der Waals* attraction items.

In BTF/MATNB, BTF/TNA, BTF/TNAZ, BTF/TNB, BTF/TNT, and BTF/CL-20 cocrystals, the proton-lone pair interactions, like C-H···O and C-H···N, are present in addition to the inter-lone-pair and lone-pair-π interactions. The proton-lone pair interactions occupy 18.6~28.7% of entire intermolecular charge population. These hydrogen bonds are 2.36~2.59 Å long and the hydrogen bond energies are up to 3.22 *kcal/mol*. As compared to the inter-lone-pair and lone-pair-π interactions, the proton-lone pair distances are roughly 20% shorter and the interactions are all attractive (Table 1). Therefore, these hydrogen bonding interactions play an indispensable role in reducing the total energy, propelling the combination of multi-component molecules into cocrystals.

**Cooperation of the intermolecular interactions and the molecular polarizability.** Interestingly, we find that the inter-lone-pair and lone-pair-π interactions can make the non-polar molecule polar, as shown in Table 2 and Fig. 2. In BTF crystal, the periodically distributed interactions break the original $C_{3h}$ symmetry of

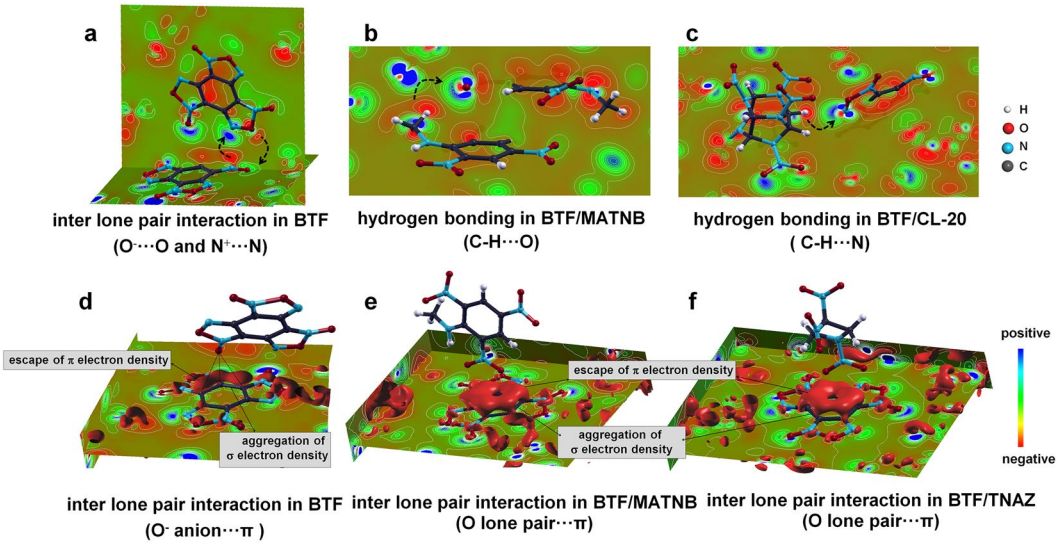


**Figure 2.** Intermolecular charge transfers due to crystal packing effect in (**a**) pristine BTF crystal, (**b**) BTF/MATNB cocrystal, and (**c**) BTF/CL-20 cocrystal. Escape of π electron density and aggregation of σ electron density at the benzene ring backbone in (**d**) pristine BTF crystal, (**e**) BTF/MATNB cocrystal, and (**f**) BTF/TNAZ cocrystal. The π electron density escape is illustrated by the isosurfaces for both pristine BTF crystal (−0.4 $e/nm^3$) and cocrystals (−0.7 $e/nm^3$).

the charge distribution in a free BTF molecule. The Mulliken population of the carbon atoms in the benzene ring decreases from 3.83 *e* to 3.81 *e* and that around the O atom in the at the border of the oxofurazan ring increases from 6.46 *e* to 6.49 *e*. Therefore, two thirds of the three $N^+$-$O^-$ bonds become more polar whereas the left one third less polar. By this way, the total dipole moment of the BTF molecule increased to ~0.3 *Debye*.

Due to the greater distinction of the electronegativity of hydrogen (2.2) from other element (oxygen: 3.5, nitrogen: 3.0, carbon: 2.6), the proton-lone pair interactions generally provoke doubled amount of charge transfer of inter-lone-pair interactions, and thus cause more increase in the molecular polarizability (Table 2 and Fig. 2). Furthermore, the presence of more electronegative nitro groups (than amine oxide group) exacerbates the escape of π electron density from the BTF molecules. By such way, the intramolecular charge distributions in the cocrystals become more anisotropic so the molecules are more polarized as compared to the pristine BTF crystal. As shown in Table 2, the dipole moment increase in the molecules of the cocrystals are between 0.7 and 1.2 *Debye*, more than in the BTF crystal (~0.3 *Debye*). Also, the TNB molecule has no dipole at the free state due to its $D_{3h}$ symmetry, but its dipole moment increases to 0.7 *Debye* when it is present in the BTF/TNB cocrystal.

**Solid-state properties of the cocrystals: thermodynamics, structure, explosion and safety.** The cooperation of the hydrogen bonding and the molecular polarizabilities increases the binding energies of the cocrystals by 19–41% as compared to the pure BTF crystal, as shown in Fig. 3 and Table 3. The increase of the binding energies implies that the multicomponent association is thermodynamically more stable as compared to the pristine crystal.

From the structural point of view, the packing coefficient (PC) of a solid is determined by the competition of two factors: compatibility and intermolecular binding energy. Similar polarizability is known to increase the solubility of two types of ingredient molecules. The pristine BTF crystal has the lowest PC of 72.02% because its binding energy is the lowest, at 14.21 kcal/mol. Whereas, for BTF/CL-20 cocrystal, although the binding energy is up to 19.77 kcal/mol, the large difference between the polarizabilities of BTF molecule and CL-20 molecule cuts off the intermolecular compatibility in crystal packing [Supplementary Fig. S3], leading to a smaller PC of 72.39%.

Our calculations indicate that the detonation performances of the cocrystals are altered over the pristine crystals due to the inter-multicomponent coupling interactions. Bulk density is a recognized criterion of detonation performances of high-energy-density substances. Although the introduction of hydrogen element in the cocrystals benefits intermolecular attractions, thus helping to denser molecular packing in space, but it is not conducive to the improvement of bulk density due to its small mass. Therefore, the bulk density of hydrogen-free BTF crystal and those of the hydrogen-including cocrystals of BTF/MATNB, BTF/TNA, BTF/TNAZ, BTF/TNB, and BTF/TNT are similar. For the detonation performance of pure BTF crystal, the heat of explosion, explosion temperature, velocity of detonation, and detonation pressure are 1474 *kcal/kg*, 5268 *K*, 8.05 *km/s*, and 29.78 *GPa*, respectively, showing satisfactory agreement with the experiments, as shown in Table 3. The BTF/CL-20 cocrystal owns similar bulk density but much improved oxygen balance as compared to pure BTF solid. Therefore, its detonation performances are significantly ameliorated, with the velocity of detonation improved by ~10% and detonation pressure improved by ~5%, respectively (Table 3).

Another multicomponent molecular packing effect is the reduced sensitivity to external stimuli of these energetic cocrystals, manifested in the strengthening of all the chemical reaction trigger linkages as compared to their

| Types | | BTF crystal | | BTF/MATNB | | BTF/TNA | | BTF/TNAZ | | BTF/TNB | | BTF/TNT | | BTF/CL-20 | |
|---|---|---|---|---|---|---|---|---|---|---|---|---|---|---|---|
| | | *D* | *S* | *D* | *S* | *D* | *S* | *D* | *S* | *D* | *S* | *D* | *S* | *D* | *S* |
| BTF-BTF | N···N | 2.98 | +1.15 | 3.06 | +1.84 | 3.01 | +1.61 | 3.26 | +0.23 | 3.12 | +1.38 | 2.95 | +2.30 | — | — |
| | O···C | 2.99 | +0.69 | — | — | 3.09 | +0.69 | — | — | 3.09 | +0.46 | 3.11 | +0.69 | 2.84 | +1.15 |
| | O···O | 2.93 | +0.69 | 2.86 | +1.38 | — | — | 3.02 | +1.84 | 3.02 | +0.69 | 3.07 | +0.69 | — | — |
| | O···N | 3.03 | +1.61 | 3.10 | +0.92 | 3.06 | +0.69 | 3.10 | +0.69 | 3.04 | +1.15 | 3.01 | +0.92 | — | — |
| BTF-Coformer | **H···O** | – | – | **2.42** | **−1.38** | **2.40** | **−1.61** | **2.43** | **−0.92** | **2.57** | **−1.15** | **2.54** | **−1.15** | **2.47** | **+0.23** |
| | **H···N** | — | — | — | — | — | — | — | — | — | — | **2.58** | **+0.69** | **2.47** | **−3.22** |
| | O···C | — | — | 3.02 | +0.46 | 2.93 | +1.15 | 2.67 | +0.69 | 2.98 | +0.46 | — | — | 3.01 | +0.69 |
| | O···O | — | — | 2.86 | +1.61 | 2.87 | +1.15 | 2.77 | +1.15 | — | — | — | — | 2.81 | +1.61 |
| | O···N | — | — | — | — | 2.96 | +0.23 | 2.66 | +0.23 | 2.89 | +1.38 | 2.88 | +0.23 | 2.89 | +1.38 |
| Coformer-Coformer | **H···O** | — | — | **2.49** | **−2.53** | **2.59** | **−0.46** | — | — | **2.36** | **−1.38** | **2.59** | **−0.92** | **2.44** | **−1.38** |
| | O···C | — | — | — | — | — | — | — | — | 3.08 | +0.69 | 3.08 | +1.15 | 3.03 | +0.92 |
| | O···O | — | — | — | — | — | — | — | — | 2.98 | +0.92 | — | — | 2.91 | +0.69 |
| | O···N | — | — | 2.91 | +0.69 | — | — | — | — | — | — | 2.90 | +0.23 | 2.94 | +0.23 |

**Table 1.** Distances (*D*, in Å) and strengths (*S*, in *kcal/mol*) of the intermolecular interactions due to crystal packing effect. The hydrogen bonding interactions are marked by the bold. The information of covalent bonds is given in supplementary Table S2. The hydrogen bonding interactions are marked by the bold. The information of covalent bonds is given in supplementary Table S2.

| | Isolate | BTF crystal | BTF/MATNB | BTF/TNA | BTF/TNAZ | BTF/TNB | BTF/TNT | BTF/CL-20 |
|---|---|---|---|---|---|---|---|---|
| BTF | 0.0 | 0.3 (↑) | 0.7 (↑) | 0.9 (↑) | 0.2 (↑) | 1.2 (↑) | 0.8 (↑) | 0.7 (↑) |
| MATNB | 5.2 | | 6.8 (↑) | | | | | |
| TNA | 2.4 | | | 3.6 (↑) | | | | |
| TNAZ | 1.6 | | | | 1.6 | | | |
| TNB | 0.0 | | | | | 0.7 (↑) | | |
| TNT | 2.0 | | | | | | 3.6 (↑) | |
| CL-20 | 0.9 | | | | | | | 2.4 (↑) |

**Table 2.** Enhancements of molecular polarizabilities (in *Debye*) due to multicomponent molecular packing effect in the seven studied systems.

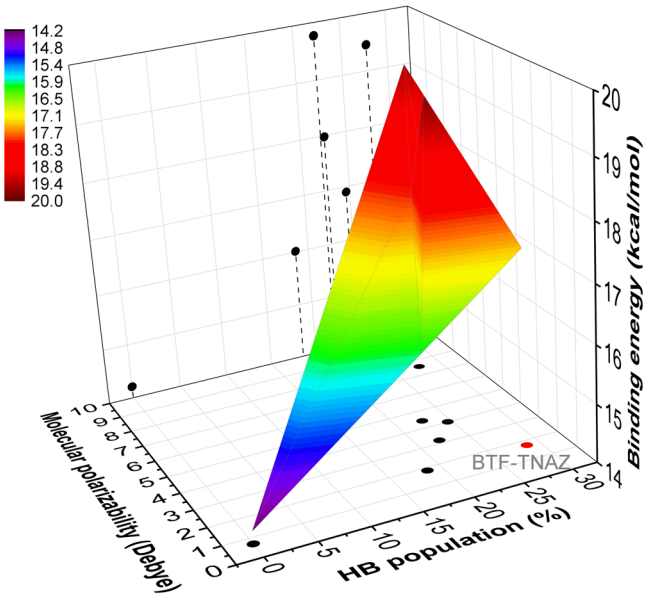


**Figure 3.** Cooperation of hydrogen bonding and molecular polarizability in increasing intermolecular binding energies (in *kcal/mol*) of the multiple-component molecular associations. The contribution of hydrogen bonding is represented by its charge proportion occupied in the Hirshfeld surfaces.

| | BTF | BTF/MATNB | BTF/TNA | BTF/TNAZ | BTF/TNB | BTF/TNT | BTF/CL-20 |
|---|---|---|---|---|---|---|---|
| Binding energy | 14.21 | 19.46 | 17.98 | 17.36 | 16.01 | 16.90 | 19.77 |
| Packing coefficient | 72.02 | 72.34 | 73.55 | 75.10 | 73.21 | 73.21 | 72.39 |
| Density | 1.85 (1.90[32],1.85[33]) | 1.75 (1.80[22]) | 1.82 (1.88[22]) | 1.84 (1.83[22]) | 1.79 (1.81[22]) | 1.75 (1.81[22]) | 1.85 (1.92[25]) |
| Oxygen balance | −38.08 | −55.03 | −46.64 | −28.81 | −46.43 | −55.08 | −20.86 |
| Heat of explosion | 1474 (1410[33]) | 1325 | 1322 | 1492 | 1412 | 1389 | 1430 |
| Explosion temperature | 5268 (3700-5570[34–36])(3700-5570[34–36])5268 (3700-5570[34–36]) (3700-5570[34–36]) | 4131 | 4336 | 4888 | 4638 | 4335 | 4844 |
| Detonation pressure | 29.78 (35.1[33], 36[37]) | 25.04 | 27.34 | 32.35 | 26.94 | 25.21 | 33.31 |
| Velocity of detonation | 8.05 (8.49[33,37]) | 7.51 | 7.76 | 8.40 | 7.73 | 7.53 | 8.51 |

**Table 3.** Predicted solid-state properties of the seven systems, including binding energies (*kcal/mol*), crystal structure characters (including packing coefficient, in % and density, in $g/m^3$), chemical composition (oxygen balance, in %), detonation performance (heat of explosion, in *kcal/kg*, explosion temperature, in *K*, velocity of detonation, in *km/s*, and detonation pressure, in *GPa*). The properties of the pristine BTF crystal from experiments and other calculations are tabulated for comparison (in brackets).The properties of the pristine BTF crystal from experiments and other calculations are tabulated for comparison (in brackets).

| | Isolate | BTF | BTF/MATNB | BTF/TNA | BTF/TNAZ | BTF/TNB | BTF/TNT | BTF/CL-20 |
|---|---|---|---|---|---|---|---|---|
| BTF ($N^+$-O) | −42.09 | −45.31(↑) | −46.92(↑) | −46.23(↑) | −43.70(↑) | −45.77(↑) | −45.54(↑) | −45.54(↑) |
| MATNB (C-$NO_2$) | −101.89 | | −110.17(↑) | | | | | |
| TNA (C-$NO_2$) | −103.96 | | | −106.72(↑) | | | | |
| TNAZ (N-$NO_2$) | −99.36 | | | | −109.71(↑) | | | |
| TNAZ (C-$NO_2$) | −91.77 | | | | −93.84(↑) | | | |
| TNB (C-$NO_2$) | −97.52 | | | | | −99.82(↑) | | |
| TNT (C-$NO_2$) | −97.29 | | | | | | −100.74(↑) | |
| CL-20 (N-$NO_2$) | −102.81 | | | | | | | −109.94(↑) |
| $h_{50\%}$ | | 21[22] | <17.8[22] | <17.8[22] | <12.6[22] | 42.2[22] | 36.2[22] | — |

**Table 4.** Enhanced strengths (*kcal/mol*) of the trigger linkages of chemical reaction initiation as compared to their counterparts in gas. The trigger linkages are $N^+$-O covalent bonds in the oxofurazan ring of BTF molecule, C-$NO_2$ bonds in nitro compound molecules, and N-$NO_2$ bonds in nitroamine molecules, and they are denoted by red crosses in Fig. 1. The $h_{50\%}$ (in *cm*) of these crystals obtained in the impact tests are as listed for comparison.The trigger linkages are $N^+$-O covalent bonds in the oxofurazan ring of BTF molecule, C-$NO_2$ bonds in nitro compound molecules, and N-$NO_2$ bonds in nitroamine molecules, and they are denoted by red crosses in Fig. 1. The $h_{50\%}$ (in *cm*) of these crystals obtained in the impact tests are as listed for comparison.

pure crystal and gas counterparts (Table S1). Here the assumption is that all the absorbed energies from external stimuli are devoted to alter the vibrational modes of the weakest covalent bonds.

For BTF crystal, the chemical reaction trigger linkages are the three $N^+$-O covalent bonds in the oxofurazan ring and their strengths are 2.53 *kcal/mol*, 3.22 *kcal/mol*, and 4.14 *kcal/mol*, respectively, higher than the gaseous BTF molecule (Supplementary Table S1 and Fig. S4). Such strengthening effect is proved to be more pronounced in the hydrogen-including systems. As shown in Table 4, the bond strengths increase by 2.07~8.28 *kcal/mol* for N-$NO_2$ and by 7.13~10.35 *kcal/mol* for C-$NO_2$.

For BTF/TNB and BTF/TNT cocrystals, the enhancement of the trigger linkages over the pure BTF crystal (by 0.46 *kcal/mol* and 0.23 *kcal/mol*, respectively) indicates their reduced sensitivities, well confirmed by the measured $h_{50\%}$ (21 *cm* for BTF, 42.2 *cm* for BTF/TNB and 36.2 cm for BTF/TNT[22]) as shown in Table 4. This result implies that the solid nature of the cocrystal is not a simple combination of the pure crystalline properties of its constituents. Nonlinear effects like the coupling of the hydrogen bonding and molecular polarizability may give the cocrystal improved sensitivity than any of its pure compounds. Whereas, the inconsistent sensitivity prediction between the calculation and the experiments for the BTF/MATNB and BTF/TNA cocrystals warns us that accurate assessment of the inherent sensitivity of single crystal (defect free), from both experimental and computational perspectives, remains a challenging task to be explored.

To conclude, we have predicted the solid nature of six novel energetic cocrystals using quantum chemical method and discovered an interesting coupling of hydrogen bonding and molecular polarizability. Their cooperation significantly enhances the stability of the multicomponent molecular association, alters the crystal packing characteristics and improves the detonation performance and the safety of the cocrystal solid as compared to their pristine compounds. Therefore, in order to rationally design improved energetic cocrystals, the heterogeneous molecular coupling effects must be taken into account.

**Methodology.** *General information.* All the calculations were performed using the recently developed density functional theory (DFT) HASEM package[27,28]. The generalized gradient approximation was used for the exchange-correlation functional in the Perdew-Burke-Ernzerhof form. Norm-conserving pseudopotentials specialized for high-energy-density molecular crystals were used to replace the core electrons. The valence electrons were described by linear combinations of numerical pseudoatomic orbitals. The reliability of this method to predict the intermolecular interaction energies and to predict the nature of high-energy-density molecular crystals has been confirmed in the previous work[27,29–31].

*Structural optimization.* Taking the information obtained from X-ray diffraction analysis as input[22,23,32], the geometry optimizations for the crystal lattices and atomic positions of BTF, BTF/MATNB, BTF/TNA, BTF/TNAZ, BTF/TNB, BTF/TNT, and BTF/CL-20 cocrystals were performed on the basis of conjugate gradient method (Fig. 1). The simulated structures were considered as finally optimized when the stress components were less than 0.01 GPa and the residual forces were less than 0.03 eV/Å. For all the studied seven systems, the calculated structures showed satisfactory agreement with the experiments: the discrepancies of the lattice parameters ranged from −2.03% to +2.82% and that of the volumes ranged from −0.51% to 3.74% (Supplementary Fig. S1).

*Characterization of solid nature.* Based on the optimized structures of the seven systems, the intermolecular charge transfers, inter-/intra-molecular interaction strengths, molecular polarizabilities, bulk density, packing coefficient, and binding energies were calculated to characterize the crystal packing effect. The detailed calculation methods are provided in the supporting information. The predicted macro solid properties include detonation performances and sensitivities to accidental initiation of detonation. For the prediction of the detonation performance, we used a recently developed method by taking into account of the statistical correction from experimental data, which were detailed in our previous work[29] (Supplementary Fig. S5). The nature of BTF has already been clarified by plenty of experimental tests and simulations and these acquired data are in turn used to confirm the reliability of the current predictions.

## Data Availability

The source data that support the plots in this Article and the other findings of this study are available from the corresponding authors upon reasonable request.

## References


1. Spitzer, D. *et al*. Continuous engineering of nano-cocrystals for medical and energetic applications. *Sci. Rep.* **4**, 6575 (2014).
2. Landenberger, K. B., Bolton, O. & Matzger, A. J. Energetic-Energetic Cocrystals of Diacetone Diperoxide (DADP): Dramatic and Divergent Sensitivity Modifications via Cocrystallization. *J. Am. Chem. Soc.* **137**, 5074 (2015).
3. Bolla, G. & Nangia, A. Pharmaceutical cocrystals: walking the talk. *Chem. Commun. (Cambridge, U. K.)* **52**, 8342 (2016).
4. Zhang, J., Parrish, D. A. & Shreeve, J. M. Curious cases of 3,6-dinitropyrazolo[4,3-c]pyrazole-based energetic cocrystals with high nitrogen content: an alternative to salt formation. *Chem. Commun. (Cambridge, U. K.)* **51**, 7337 (2015).
5. Cherukuvada, S. & Nangia, A. Eutectics as improved pharmaceutical materials: design, properties and characterization. *Chem. Commun. (Cambridge, U. K.)* **50**, 906 (2014).
6. Snyder, C. J. *et al*. Simple and Efficient Synthesis of Explosive Cocrystals containing 3,5-Dimethylpyrazol-1-yl-substituted-1,2,4,5-tetrazines. *Chemistry* **23**, 16466 (2017).
7. Sabin, J. R. *Advances in Quantum Chemistry*. (Academic Press, 2014).
8. Shukla, M. K., Boddu, V. M., Steevens, J. A., Damavarapu, R. & Leszczynski, J. *Energetic Materials: From Cradle to Grave*. (Springer International Publishing, 2017).
9. Desiraju, G. R. Crystal and co-crystal. *CrystEngComm* **5**, 466 (2003).
10. Bond, A. D. What is a co-crystal? *CrystEngComm* **9**, 833 (2007).
11. Bolton, O., Simke, L. R., Pagoria, P. F. & Matzger, A. J. High Power Explosive with Good Sensitivity: A 2:1 Cocrystal of CL-20:HMX. *Cryst. Growth Des.* **12**, 4311 (2012).
12. Weinan, E. *Principles of Multiscale Modeling*. (Cambridge University Press, 2011).
13. Huang, R.-Y. & Xu, H. Comment on Synthesis and characterization of the pentazolate anion cyclo-$N_5^-$ in $(N_5)_6(H_3O)_3(NH_4)_4Cl$. *Science* **359**, eaao3672 (2018).
14. Zhou, H., Ma, Z.-l, Wang, J.-l & Wang, D. Theoretical study of an energetic material di-1H-1,3,4-triazole derivatives. *Def. Technol.* **10**, 384 (2014).
15. Tsyshevsky, R. V., Pagoria, P. & Kuklja, M. M. Searching for new energetic materials: Computational design of novel nitro-substituted heterocyclic explosives. *AIP Conference Proceedings* **1793**, 030028 (2017).
16. Sinditskii, V. P., Kolesov, V. I., Egorshev, V. Y., Patrikeev, D. I. & Dorofeeva, O. V. Thermochemistry of cyclic acetone peroxides. *Thermochim. Acta* **585**, 10 (2014).
17. Dearden, J. C., Rotureau, P. & Fayet, G. QSPR prediction of physico-chemical properties for REACH. *SAR and QSAR in Environmental Research* **24**, 279 (2013).
18. Fayet, G., Rotureau, P., Prana, V. & Adamo, C. Global and local quantitative structure–property relationship models to predict the impact sensitivity of nitro compounds. *Process Saf. Prog.* **31**, 291 (2012).
19. Hutchison, G. R., Ratner, M. A. & Marks, T. J. Intermolecular Charge Transfer between Heterocyclic Oligomers. Effects of Heteroatom and Molecular Packing on Hopping Transport in Organic Semiconductors. *J. Am. Chem. Soc.* **127**, 16866 (2005).
20. Sutton, C., Risko, C. & Brédas, J.-L. Noncovalent Intermolecular Interactions in Organic Electronic Materials: Implications for the Molecular Packing vs Electronic Properties of Acenes. *Chem. Mater.* **28**, 3 (2016).
21. Ma, Y. *et al*. Crystal Packing of Low-Sensitivity and High-Energy Explosives. *Cryst. Growth Des.* **14**, 4703 (2014).
22. Zhang, H. *et al*. Five Energetic Cocrystals of BTF by Intermolecular Hydrogen Bond and pi-Stacking Interactions. *Cryst. Growth Des.* **13**, 679 (2013).
23. Yang, Z. *et al*. Characterization and Properties of a Novel Energetic-Energetic Cocrystal Explosive Composed of HNIW and BTF. *Cryst. Growth Des.* **12**, 5155 (2012).
24. Sun, C. Q., Chen, J., Gong, Y., Zhang, X. & Huang, Y. (H, Li)Br and LiOH solvation bonding dynamics: Molecular Nonbond Interactions and Solute Extraordinary Capabilities. *J. Phys. Chem. B* **122**, 1228 (2018).
25. Sun, C. Q. & Sun, Y. In *Chem. Phys.* Vol. **113** (eds Albert W. Castleman, Jan Peter Toennies, Kaoru Yamanouchi, & Wolfgang Zinth) (Springer, 2014).
26. Sun, C. Q. *Relaxation of the Chemical Bond: Skin Chemisorption Size Matter ZTP Mechanics $H_2O$*. (Springer, 2014).

27. Zhang, L. *et al*. Phase Transition in Octahydro-1,3,5,7-tetranitro-1,3,5,7-tetrazocine (HMX) under Static Compression: An Application of the First-Principles Method Specialized for CHNO Solid Explosives. *J. Phys. Chem. B* **120**, 11510 (2016).
28. Mo, Z. *et al*. JASMIN: a parallel software infrastructure for scientific computing. *Front. Comput. Sci. China* **4**, 480 (2010).
29. Zhang, L., Wu, J.-Z., Jiang, S.-L., Yu, Y. & Chen, J. From intermolecular interactions to structures and properties of a novel cocrystal explosive: a first-principles study. *Phys. Chem. Chem. Phys.* **18**, 26960 (2016).
30. Jiang, C. *et al*. Response to Comment on Synthesis and characterization of the pentazolate anion cyclo-$N_5^-$ in $(N_5)_6(H_3O)_3(NH_4)_4Cl$. *Science* **359**, eaas8953 (2018).
31. Zong, H.-H. *et al*. Structural, mechanical properties and vibrational spectra of LLM-105 under high pressures from a first-principles study. *J. Mol. Model.* **23**, 275 (2017).
32. Cady, H. H., Larson, A. C. & Cromer, D. T. The Crystal Structure of Benzotrifuroxan (hexanitrosobenzene). *Acta Cryst.* **20**, 336 (1966).
33. Akst, I. B. Heat of detonation, the cylinder test, and performance munitions in *9th International Symposium on Detonation*. (Portland, 1989).
34. Dolgoborodov, A., Brazhnikov, M., Makhov, M., Gubin, S. & Maklashova, I. Detonation performance of high-dense BTF charges. *J. Phys. Conf. Ser*. **500**, 052010 (2014).
35. Dolgoborodov, A. Y., Brajnikov, M. A., Makhov, M. N., Safronov, N. E. & Kirilenko, V. G. Detonation parameters of pressed charges of benzotrifuroxane. *Combustion, Explosion, and Shock Waves* **49**, 723 (2013).
36. Keshavarz, M. H. Correlations for predicting detonation temperature of pure and mixed CNO and CHNO explosives. *Indian J. Eng. Mater. Sci.* **12**, 158 (2005).
37. Hobbs, M. L. & Baer, M. R. Calibration of the BKW-EOS with a Large Product Species Data Base, Measured CJ Properties in *the 10th Symposium (International) on Detonation*. (Boston, 1993).



## Acknowledgements
This work was supported by the National Natural Science Foundation of China through Grant No. 11604017. L.Z. thank Prof. CQ Sun, Prof. ML Yang, Dr. YS Wen, and Ms. HH Zong for discussion.


## Author Contributions
L.Z., S.J. and J.C. conceived the theory and designed the calculations. S.J. and Y.Y. developed all the used DFT methods. All authors contributed to the overall scientific interpretation.

## Additional Information
**Supplementary information** accompanies this paper at https://doi.org/10.1038/s41598-018-37500-y.

**Competing Interests:** The authors declare no competing interests.

**Publisher's note:** Springer Nature remains neutral with regard to jurisdictional claims in published maps and institutional affiliations.


**Open Access** This article is licensed under a Creative Commons Attribution 4.0 International License, which permits use, sharing, adaptation, distribution and reproduction in any medium or format, as long as you give appropriate credit to the original author(s) and the source, provide a link to the Creative Commons license, and indicate if changes were made. The images or other third party material in this article are included in the article's Creative Commons license, unless indicated otherwise in a credit line to the material. If material is not included in the article's Creative Commons license and your intended use is not permitted by statutory regulation or exceeds the permitted use, you will need to obtain permission directly from the copyright holder. To view a copy of this license, visit http://creativecommons.org/licenses/by/4.0/.

© The Author(s) 2019